Biomaterials Science

Cyclic Strain Enhances the Early Stage Mineral Nucleation and the Modulus of Demineralized Bone Matrix

Journal:	*Biomaterials Science*
Manuscript ID	BM-ART-06-2021-000884
Article Type:	Paper
Date Submitted by the Author:	07-Jun-2021
Complete List of Authors:	Kim, Doyoon; Washington University in St Louis, Department of Energy, Environmental and Chemical Engineering Lee, Byeongdu; Argonne National Laboratory Advanced Photon Source, X-ray Sciences Division Marshall, Brittany; Columbia University, Department of Orthopedic Surgery, Department of Biomedical Engineering, Thomopoulos, Stavros; Columbia University, Department of Orthopedic Surgery, Department of Biomedical Engineering Jun, Young-Shin; Washington University in St Louis, Energy, Environment and Chemical Engineering

SCHOLARONE™
Manuscripts

Cyclic Strain Enhances the Early Stage Mineral Nucleation and the Modulus of Demineralized Bone Matrix†

Doyoon Kim[1‡], Byeongdu Lee[2], Brittany Marshall[3], Stavros Thomopoulos[3], and Young-Shin Jun[1*]

[1]*Department of Energy, Environmental & Chemical Engineering, Washington University in St. Louis, St. Louis, Missouri 63130, United States*

[2]*X-ray Science Division, Argonne National Laboratory, Argonne, Illinois 60439, United States*

[3]*Department of Orthopedic Surgery, Department of Biomedical Engineering, Columbia University, New York, New York 10032-3072, United States*

*To Whom Correspondence Should be Addressed

Address: One Brookings Drive, Campus Box 1180

E-mail: ysjun@wustl.edu

http://encl.engineering.wustl.edu/

† Electronic supplementary information (ESI) available

‡ Current address: Department of Civil and Environmental Engineering, Massachusetts Institute of Technology, Cambridge, MA 02139, USA

Abstract

The adaptive response of bones to mechanical loading is essential for musculoskeletal development. Despite the importance of collagen in bone mineralization, little is known about how cyclic strain influences physicochemical responses of collagen, especially at the early stage of mineralization when the levels of strain are higher than those in mature bones. The findings in this study show that, without any cell-mediated activity, cyclic strain increases nucleation rates of calcium phosphate (CaP) nanocrystals in highly-organized collagen matrices. The cyclic strain enhances the transport of mineralization fluids with nucleation precursors into the matrix, thus forming more CaP nanocrystals and increasing the elastic modulus of the collagen matrix. The results also suggest that the multiscale spatial distribution of nanocrystals in the fibrous collagen network determines tissue-level mechanical properties more critically than the total mineral content. By linking nano- and micro-scale observations with tissue-level mechanical properties, we provide new insights into designing better biomaterials.

1. Introduction

Bones have hierarchical structures that consist mainly of an organic fibrillar template, an inorganic mineral, and cells.[1] Type I collagen, the primary extracellular protein in bone, provides the fibrillar template for deposition of calcium phosphate (CaP) nanocrystals known as bioapatite (an analog of hydroxyapatite, HA).[2] The nanoscale through microscale organization of collagen fibrils and CaP nanocrystals determines tissue-level mechanical behaviors of bones.[3,4] For example, bovine tibias have relatively high concentrations of CaP mineral to support high body weight, whereas tortoise femurs with higher porosity and low mineralization degree are light and flexible.[5–7]

The biological control of collagen mineralization has been extensively studied and is dictated mainly by osteoblasts, which function in groups of connected cells during bone formation.[1] During mineralization, osteoblasts become entrapped by the mineralized collagen matrix and fully differentiate into mature bone cells called osteocytes; these cells are then interconnected by channels called canaliculi, allowing them to communicate with each other to control tissue-level bone properties.[2] Physiologic mechanical loads are also known drivers of bone formation and remodeling.[8] For example, mechanical loading from physical activity increases bone mineral density in young children.[9] Mechanobiology studies have shown that cells respond to strain-mediated fluid flow under natural cyclic loading environments[10] to increase bone formation rates.[11] For example, Piekarski and Munro suggested that deformations of bones caused by mechanical loading generate fluid flow, thereby promoting nutrient delivery to the osteocytes and removing their waste products.[12] Their suggestion was supported by later studies showing that bone cells respond sensitively to fluid shear stress,[10] leading to increased intracellular concentrations of calcium ions in bone cells[13] and inhibition of osteoclast formation.[14]

In addition to biological factors, more recent studies have emphasized the roles of physicochemical collagen structure in bone mineralization by evaluating the direct surface

interaction between collagen fibrils and CaP nuclei in the absence of any cellular activity.[15–21] For example, several studies successfully reproduced in vitro intrafibrillar collagen mineralization using polyaspartic acid (pAsp), which simulated non-collagenous proteins in physiological conditions. [18,20,21] Polyanionic peptides, such as pAsp are known to contribute to intrafibrillar mineralization by forming an amorphous precursor with fluidic characteristics[18,20,21] and by preventing undesirable extrafibrillar nucleation.[16,17] Furthermore, Wang et al. showed an in vitro formation of hierarchically-ordered mineralized collagen fibrils mimicking a bone structure without any cell activity or non-collagenous proteins.[19] Based on in situ observations and a modified version of classical nucleation theory, our previous study also revealed that the nanoscale geometry of the collagen gap regions could significantly reduce energy barriers to intrafibrillar mineralization, emphasizing an active role of collagen in nucleation, which previously had underestimated compared to biological factors.[16] Although these findings illuminated physicochemical aspects of bone mineralization, it remains unclear whether mechanical loading also affects strain-induced collagen mineralization at their early stages without any cellular activities.

In the current study, we investigated the influence of cyclic strain on the early stage mineralization of collagen matrices extracted by demineralizing chicken tibia bones. We determined the nucleation rates and crystalline phases of CaP nanocrystals during in situ mineralization, using small-angle X-ray scattering (SAXS) and wide-angle X-ray diffraction (WAXD). Compared to static loading or control (unloaded) conditions, cyclic loading guides more CaP nanocrystals to be deposited inside the collagen matrix, with a faster nucleation rate through increased transport of mineralization fluid. The nanocrystals formed inside the collagen matrix (dominant under cyclic strain) contribute to matrix elastic moduli more effectively than those formed outer surfaces of the matrix (dominant under static strain). The findings of this study highlight the importance of nano- and microscale mineral distribution,

over a total mineral volume fraction-based traditional model, to accurately evaluate tissue-level mechanical properties.

2. Experimental

2.1. Preparation of collagen samples

Tibia bones were separated from fresh chicken legs obtained from a local grocery store (Whole Foods Market, St. Louis, MO). Top and bottom metaphysis and epiphysis of the bones were removed from the tibia using a diamond saw. The soft tissues, bone marrow, and blood were also carefully drawn, leaving hollow-shaft like bones. The bone shafts were demineralized in ethylenediaminetetraacetic acid (EDTA) solution (0.1 M, pH 7.4) for three weeks under magnetic stirring (130 rpm) at room temperature. The solution was replaced every two days. The remaining soft collagen parts of the bones, which might contain a small fraction of inherent non-collagenous proteins such as osteocalcin and osteopontin,[22] were cut in half longitudinally using scissors. Because this digestion process may cause an adverse effect on collagen structure by unraveling microfibril bundles,[23] we avoided the artificial removal of non-collagenous proteins from the collagen matrices. The obtained matrices represented the dense and well-organized fibrillar collagen structure seen in cortical bones.[24] The half-tubular demineralized bones were sectioned on a freezing stage (Physitemp BFS-30MP) using a sledge microtome (Leica 1400) to obtain thin and flat collagen samples with thicknesses < 1 mm. Using a razor blade, collagen samples were cut in a uniform shape 0.5 cm wide × 3 cm long for further experiments. The thickness of each matrix before application of strain condition was accurately measured using a laser scanner (LJ-V700-1, Keyence) and this information is used for mechanical evaluation.

2.2. In situ X-ray data collection during collagen mineralization

To mineralize collagen samples under strain conditions, we built a stainless steel holder (Fig. S1a†). During mineralization up to 10 h, the holder, containing two collagen samples, was

placed in 130 mL of the modified simulated body fluid (m-SBF, Table S1†). With 2.5 times higher Ca and P concentration than normal SBF and the addition of 10 mg mL^{-1} pAsp,[16–18,21] m-SBF resulted in vitro collagen mineralization sufficient for further analysis within 10 h. This holder was connected to a customized motor-driven BiSlide module (Velmex, Inc.) to control the strain during mineralization (Fig. S1b†). To collect in situ X-ray data, mineralization was conducted at the Advanced Photon Source at Argonne National Laboratory (Argonne, IL, USA). Every two hours during mineralization, the collagen-loaded sample holder was detached from the BiSlide module and then moved to a specially designed sample stage for SAXS measurements (Fig. S1c†), after which the holder was promptly re-attached to the module for further mineralization. Collagen matrices were rinsed with phosphate buffer to exclude possible attachment of CaP crystals formed in solution before the measurement. During each measurement, the mineralization reaction was interrupted for less than 5 minutes. The same experiments were repeated for WAXD measurements at Sector 11 ID-B. The detailed procedures are described in Supporting Note†.

2.3. Ex situ imaging

Collagen matrices were fixed in 100 mM cacodylate buffer containing 2% paraformaldehyde and 2.5% glutaraldehyde. The matrices were then fixed with 1% osmium tetroxide for 1 h. After dehydration in successive ethanol baths, samples were embedded in epoxy resin, and thin sections (95–100 nm) were prepared using an ultramicrotome. Uranyl acetate and Reynold's lead citrate were used for staining. The stained sections were imaged using transmission electron microscopy (TEM) at an accelerating voltage of 100 kV (JEOL 1200 EX II). Collagen matrices were also analyzed by scanning electron microscopy (SEM) equipped with energy-dispersive X-ray spectroscopy (EDS) (FEI Nova NanoSEM 2300). After mineralization experiments, samples were soaked in an ethanol bath for more than 5 h for fixing and removing excess ions. Then, matrices were frozen in liquid nitrogen and cut into ~1 mm thick using a razor blade for cross-sectional imaging. The cross-sectioned

samples were placed on SEM stubs and sputter-coated with Au-Pd under Ar at 0.2 mbar (Cressington 108) to increase conductivity, then imaged with a 10 kV electron accelerating voltage at a 5–6 mm working distance.

Confocal microscope (ZEISS LSM880) images were obtained from collagen matrices exposed to different mechanical loading conditions in phosphate buffer saline (PBS) containing 2% of PicroSirius Red F3BA stain solution (Polysciences, Inc) for 10 h. The stained collagen matrices were thoroughly rinsed with PBS to remove excess PicrosSirius Red, then imaged at different confocal sections with 3 μm steps at the same microscope operation parameters (×20 lens, 200×200 μm^2 scanning area with fixed exposure time, 543 nm laser, DsRed filter). Fluorescence images were not corrected for the reducing intensities along the depth of confocal sections to avoid any unintentional change of the data during the post process.

2.4. Mechanical testing

Uniaxial tensile testing was conducted at the Musculoskeletal Soft Tissue Lab, Washington University in St. Louis. Collagen matrices mineralized under different strain conditions were loaded in a custom-designed planar tensile test machine (TestResources, Shakopee). Both ends of samples were clamped at the actuators of the machine and pulled in tension at a rate of 1% elongation per second until failure while tensile stress was monitored. The monitored load-displacement relationship was used for further evaluation of mechanical properties of samples, such as elastic modulus (E), strength, resilience, and yield strains.

2.5 Statistical analyses

Quantitative data are given as mean ± standard error. The error bars in the graphs represent standard errors. The variable n indicates the number of samples analyzed. Neither the experiments nor the outcomes were blinded during the study. Statistical differences were determined using one-way ANOVA with the Tukey HSD post-hoc test, with significance considered $p < 0.05$ (R ver. 3.2.0). We used two-way ANOVA to compare the elastic

modulus, strength, and resilience of collagen matrix mineralized in PBS and m-SBF under different strain conditions.

3. Results and Discussion

3.1. Nucleation and crystallization during in situ mineralization

Nucleation and crystallization of CaP nanocrystals in collagen are necessary initial steps for bone mineralization. To provide quantitative kinetic information on nucleation and crystallization, SAXS and WAXD data were collected during in situ collagen mineralization.[16,17,25] To better quantify the nucleation rates and evaluate the morphology of newly formed particles without interference by peaks caused by the periodicity (~67 nm) of the collagen gap and hole regions, 1-dimensional scattering intensities along the scattering vector q, $I(q)$, were extracted by averaging the sector along the direction perpendicular to the fibrillar direction (Fig. S1d†). The setup was designed to test the effect of strain conditions on collagen mineralization in the following groups: 1) control (0% strain), 2) cyclic strain (3% peak strain applied at 0.5 Hz), and 3) static strain (constant 3% strain). The 0.5 Hz frequency is comparable to a slow human walking motion (30 steps per min per leg).[26] The peak physiologic strains experienced by typical mature, fully mineralized, animal bones range from 0.1 to 0.32%;[27] however, the strain levels in immature collagenous tissues at the onset of mineralization are likely an order of magnitude higher.[28] To replicate the early stages of bone mineralization when the strain levels given to collagen are expected to be high, 3% cyclic strain was applied to collagen matrices in the current study. The collagen matrices were prepared by demineralizing chicken tibias by EDTA extraction,[24] thereby providing collagen matrices as a biological template representing the fibrillar density and alignment of collagen in mineralizing cortical bone.[29] SAXS patterns of collagen matrices were not affected by three mechanical loading conditions applied for 20 h in PBS (Fig. S2†), indicating that these conditions do not damage collagen structure significantly .

The matrices were re-mineralized under three strain conditions in the m-SBF for 10 h while collecting the SAXS data. We observed that the number of newly formed particles increased over time after 4–6 hours of induction period in the mineralization solution. A similar induction period was observed for all three conditions, probably due to the use of the same m-SBF as a medium. The formation of nanocrystals appeared as increased SAXS intensities in a q range of 0.02–0.3 $Å^{-1}$, regardless of the applied strain (Fig. S3a†). The background—unmineralized collagen—subtracted patterns after this initial induction time were relatively uniform for all three conditions and fit well with a plate-like shape with a thickness of 1.5 nm (Fig. S4†). This dimension is comparable to bioapatite crystals commonly observed in nature[4,30] and during in vitro mineralization.[16,17,31] The uniform shape of nuclei over time indicates that the increasing number of nuclei (i.e., nucleation-dominant system), not the growth of individual particles, was the dominant reason for the increasing SAXS intensities in our experimental conditions.[32]

The crystallization of nuclei during in situ mineralization was also observed from WAXD measurements and compared to a fresh tibia bone and synthetic HA samples. Until 6 h, the development of WAXD intensity was weak. Thus, all the patterns were not easily distinguished from the pattern of unmineralized collagen (at 0 h, Fig. S3b†), which shows a peak corresponding to intra-amino acid spacing (d = 2.9 Å).[33] After 8 hours of mineralization, a small peak at 1.83 $Å^{-1}$ (the (002) diffraction of HA) and a small shoulder at 2.25 $Å^{-1}$ (overlap of (211) and (112) diffraction peaks of HA) appeared. These changes reveal the development of the corresponding crystallographic planes in collagen matrices (Fig. S3b†). These HA characteristic diffraction peaks appeared slightly later than the induction time observed from SAXS (4–6 h), suggesting that the nucleation is followed by crystallization, as similarly observed in our previous studies.[16,17] The mineralized collagen matrices show weak peak intensities until 10 h without orientation unlike the fresh bone sample (Fig. S5†), manifesting that collagen mineralization is still at its early stage. Background-subtracted

WAXD patterns revealed the mineral structure as poorly crystalline HA (Fig. S3c†), typical of bioapatite from most animal bones.[2] During the induction time, there was no clear evidence of the formation of amorphous calcium phosphate (ACP) in collagen matrices as an intermediate phase neither from SAXS nor WAXD. This result is consistent with our previous study reporting that the nucleation pathway involving ACP was only dominant without pAsp in unconfined extrafibrillar space,[16,17] which would not be offered by the highly-organized collagen matrix used in this study. Both SAXS and WAXD data confirmed that applied strain (cyclic and static) did not significantly affect the morphology (plate-like, uniform thickness) and crystallinity (poorly crystalline HA) of CaP nanocrystals formed during collagen mineralization at this early stage.

3.2. Cyclic strain enhances nucleation rates and elastic moduli

Using the morphology and crystalline structure of the CaP nuclei determined from SAXS and WAXD data, we calculated the particle volume fractions and nucleation rates in collagen matrices using the SAXS invariant value, $Q = \frac{1}{2\pi^2}\int q^2 I(q) dq$,[34] where $I(q)$ is 1-dimensional scattering intensities along the scattering vector q. Here, $I(q)$ was normalized by the incident beam intensity and sample thickness, and calibrated using a reference glassy carbon standard sample[35] to fairly compare the values obtained from the different measurements. This value indicates the total scattering amount and thus is proportional to particle number concentration per scanned surface area, $N_c = \frac{Q}{r_e^2 \Delta\rho^2 V}$, when the particle morphology is uniform. [34] Here, r_e and V represent the classical electron radius (2.818 fm) and the volume of an individual particle, respectively. $\Delta\rho$ is the difference in electron densities between HA and collagen ($\Delta\rho$ = 5.02×10^{23} cm^{-3}, assuming particles were HA crystals surrounded by collagen).[17,36] From the linear slopes of N_c vs. time plots (Fig. 1a), nucleation rates normalized to the scanned surface area (J_s) were obtained for each sample (Fig. 1b). The results from four different experiments (8 samples per each strain condition) showed that, compared to the unloaded condition, J_s

under cyclic strain increased by 17% and J_s under static strain decreased by 13% (the difference in Js between the cyclic and static conditions was statistically significant).

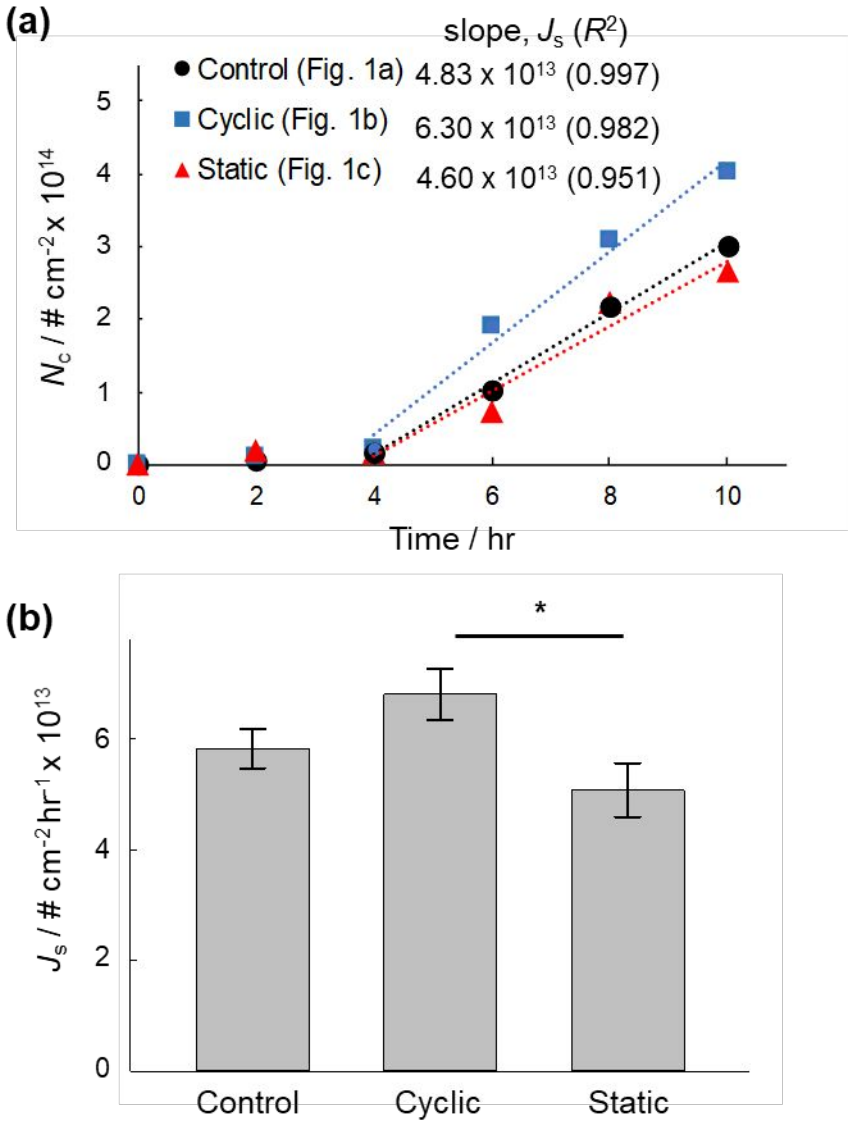

Figure 1. The influence of strain conditions on collagen mineralization. a) Slopes of linear regions of number concentrations vs. time plots to evaluate nucleation rates (J_s). The data in each plot were obtained from the one-time SAXS measurement shown in Fig. S3a†) Mean and standard errors of J_s during collagen mineralization under different strain conditions. Number of samples, n = 8 for each condition. * indicates a statistically significant difference ($p < 0.05$, one-way ANOVA with the Tukey HSD post-hoc test) for comparison under the bar.

The mechanical properties of collagen matrices mineralized under different strain conditions in m-SBF were analyzed and compared to the properties of matrices reacted in PBS, where no mineralization occurred (Fig. 2). Mineralization in m-SBF for 10 h

significantly increased the elastic modulus (E) and strength of the matrices, as determined by two-way ANOVA ($p < 0.05$, Fig. 2a,b), ruling out the possibility of significant collagen damage during mineralization under mechanical loading conditions. A slightly increasing trend in resilience by mineralization was also observed ($p = 0.052$, Fig. 2c). On the other hand, in PBS, the differences in these properties by strain condition were not significant, indicating that neither cyclic nor static strain altered the mechanical properties without mineralization. E of collagen matrices in PBS group were 79.6 ± 8.6 MPa, comparable to other demineralized bone samples such as mice femora.[37] Mineralization in m-SBF under cyclic strain increased E of the matrices by 30.9% compared to matrices reacted in PBS under cyclic strain (Fig. 2a). In contrast, E was slightly higher after mineralization in m-SBF than in PBS for the control group. The increase in E for the static condition was not easily distinguished from that of unmineralized matrices. In addition to E, samples mineralized under cyclic strain showed the highest strength and resilience, and the control group also showed noticeable increases in both properties with mineralization (Fig, 2b,c). However, the static strain condition does not change the strength and resilience after 10 h of mineralization, unlike in native bones, where E, strength, and resilience all increased with mineralization.[38]

On the other hand, yield strain was not influenced by either mineralization or strain condition (Fig. 2d). Because 3% strain was much lower than the yield strain and the strain was applied before the matrices became too brittle (i.e., decrease in yield strain),[38] there was no statistical difference in yield strain after 10 h of reaction in PBS compared to that in m-SBF (20.2 ± 0.9% and 20.5 ± 0.8%, respectively).

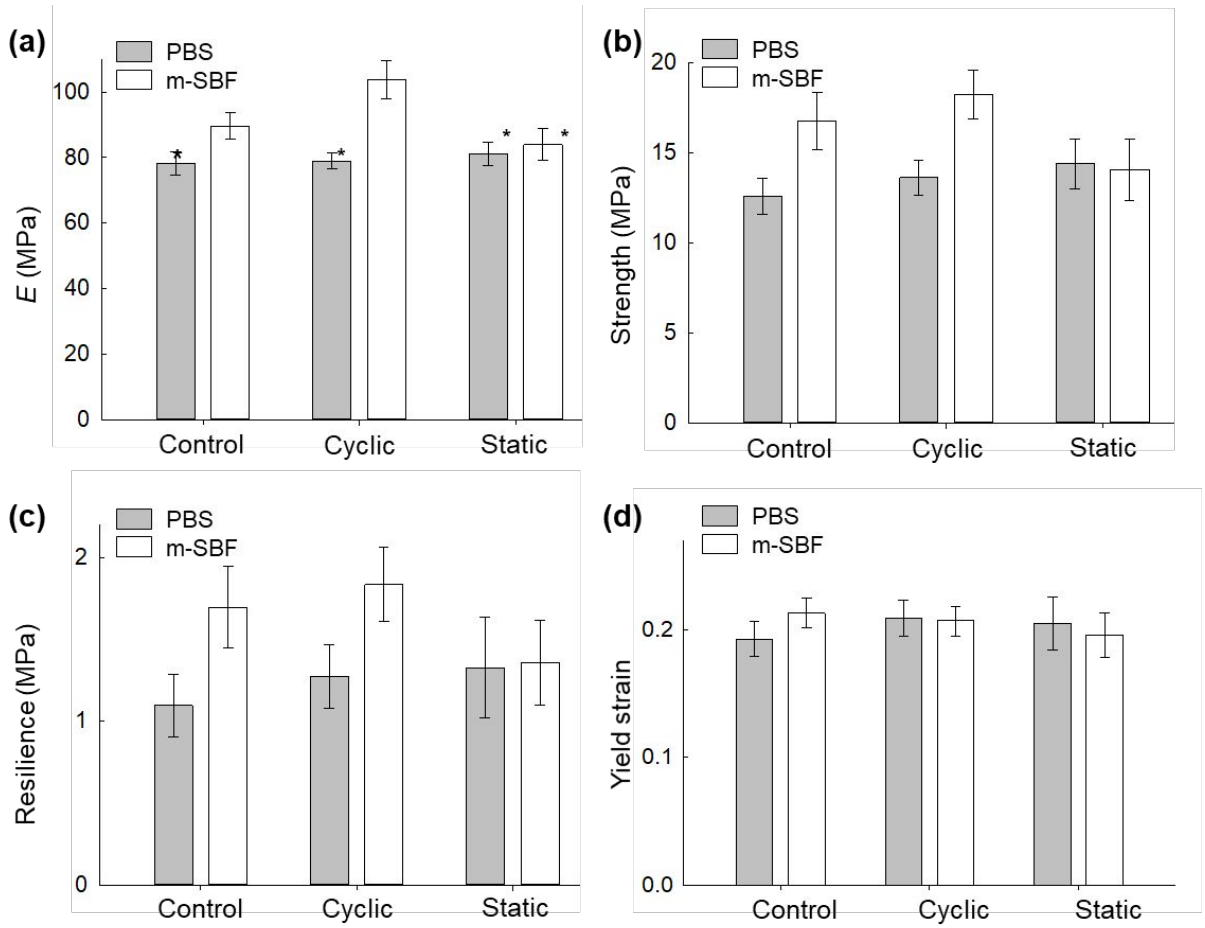

Figure 2. Tensile test results of collagen matrices. a) Elastic modulus, *E*, b) strength, c) resilience, and d) yield strain. Collagen matrices experienced different strain conditions for 10 h in PBS (no mineralization, $n = 8$ for each condition) and modified simulated body fluid (m-SBF, with mineralization, $n = 9$ for each condition). Error bars are standard errors. * indicates a statistically significant difference compared to the cyclic-SBF system ($p < 0.05$, two-way ANOVA with the Tukey HSD post-hoc test).

3.3. Spatial distribution of CaP nanocrystals under strain conditions

The mechanical testing showed that cyclic strain increased *E* more significantly than the other two conditions. This result is intriguing because there was no significant difference in the volume fractions of mineral in the collagen matrix (f_V) among the three strain groups after 10 h of mineralization (Fig. S6†). The wide variations in f_V were caused by induction time and sample thickness. Therefore, we hypothesize that CaP nanocrystals formed under cyclic loading have a different spatial distribution within collagen matrices from other groups. Further, cyclic strain conditions can alter the availability of nucleation sites and subsequent

mineral formation, leading to more effective increases in E, while simultaneously increasing J_s (Fig. 1b).

According to transmission electron microscopy (TEM) images of sample cross-sections (Fig. 3a), strain conditions affected the spatial distribution of mineral at the sub-micrometer scale (Fig. 3b–d). With f_V less than 1.4% after 10 h of mineralization (a level that represents the early stages of bone mineralization), densely mineralized areas showing dark contrast were only a few micrometers near edge of the matrices for all groups. However, the ratio of lengths of the densely mineralized areas inside (inner surface mineralization, IS) and outside (outer surface mineralization, OS) of the matrices were distinct. The IS would include CaP nanocrystals both formed inside of the collagen gap regions (i.e., intrafibrillar mineralizatoin) and thinly sheathed around the collagen (a type of extrafibrillar mineralization)[4]. In Fig. 3b–d, the yellow line indicates the interface where collagen fibrils stop appearing (red dotted rectangles), and aggregates of plate-like CaP nanocrystals start forming independently from collagen (solid black rectangles). Using the gray value profiles of these TEM images along the depth direction (z-direction in Fig. 3a), the fractions of mineralization depths for IS and OS (f_{IS} and f_{OS}) were estimated (Fig. S7†). f_{IS} was greatest (0.69) in the cyclic strain group compared to the control and static strain groups, corresponding to the highest J_s (Fig. 1b).

On the other hand, CaP aggregates independent from collagen were most dominant under the static condition ($f_{OS} = 1 - f_{IS} = 0.65$, Fig. 3d). The thickness of these CaP plates is expected to be similar to those inside the matrix, as analyzed by SAXS (~1.5 nm, Fig. S4†). Previous studies also reported a similar range of thickness from aggregated CaP plates formed in biomimetic solutions.[16,17,31] However, the long dimension of the plates (> 200 nm) was not characterized by SAXS due to the limited q range. Scanning electron microscopy with energy-dispersive X-ray spectroscopy (SEM-EDX) analyses supported that the layer of CaP aggregates on the outer surfaces of collagen matrices was most evident under static condition

(Fig. S8–S9†). This mineral layer is not expected to contribute mechanically to the collagen matrix. Still, it could just act as a diffusion barrier, preventing mineralization of the inner portion of the matrix.[17] Notably, the lowest J_s was observed under static strain (Fig. 1b), and a clear negative correlation ($R^2 = 0.78$) was observed between f_V and sample thickness (Fig. S6d†). The results indicate that the mineral layer created by static strain conditions acted as a diffusion barrier at the outer surface, decreasing J_s and limiting mineralization of the inner portion of the matrix. In contrast, cyclic strain shows higher J_s for thicker samples, because the cyclic strain condition allows the mineralization into the deeper interior space (Fig. S7c†). Thus, the application of cyclic strain can be beneficial for generating mineralizing scaled-up collagen-based biomaterials.[15,19]

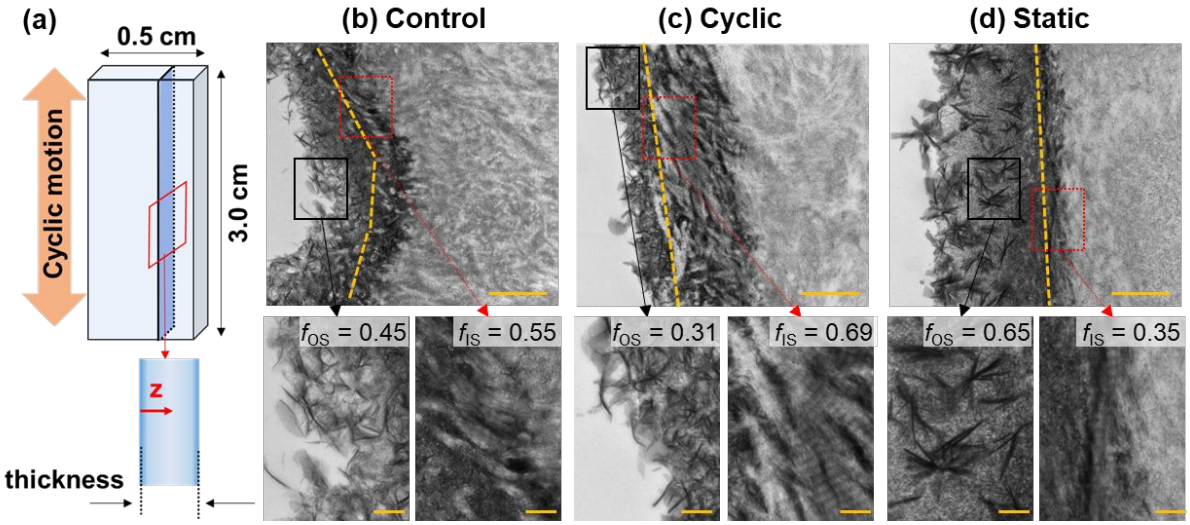

Figure 3. Cross-sectional images of collagen matrices. a) Schematic of sample geometry and sectioning plane. b-d) Transmission electron microscope images of cross-sections. Bottom panels are higher magnification images of selected areas from top panels. Scales bars in the top and panels are 1 μm and 200 nm. Yellow dotted lines indicate the interface between CaP aggregates and the outermost surface of the matrices. Highly mineralized areas in matrices near the interface show darker contrast than lightly mineralized areas. f_{IS} and f_{OS} indicates the fraction of inner surface and outer surface mineralization, respectively (See Fig. S7† for details).

3.4. Nucleation and crystallization during in situ mineralization

Previously, nanoscale models have described mechanical aspects of collagen fibrils and CaP nanocrystals during deformation;[4,39] however, few attempts have been made to correlate the location of nanocrystal deposits and the macroscale mechanical properties.[4] In this study, using a tissue-level model, we evaluated how effectively the CaP nanocrystals contribute to E, depending on their distribution, which was determined by different strain conditions. According to Smith et al., the relative increase in E can be formulated by the following relation.[40]

$$\frac{E}{E_{\mathrm{UN}}} = \exp(A\, f_{\mathrm{v}}\,(1 - 2f_{\mathrm{DP}}) \qquad (1)$$

Here, the elastic modulus of the unmineralized matrix was E_{UN} = 79.6 MPa, as obtained from the mechanical testing results of the PBS group (Fig. 2a). Volume fractions of mineral in the collagen matrix (f_{V}) values were obtained from SAXS analyses (Fig. S6†). Smith et al. derived Eq. (1) based on a previous study by Teng, which describes nonlinear bimodular stiffness properties.[41] The effectiveness of particles in load transfer can be expressed as the fraction of debonded particles (f_{DP}) among total particles formed in the matrix. A debonded particle, unlike a well-bonded particle, poorly contacts the surface of the pores, and thus cannot transfer load within the matrix, negatively influencing E. The constant A is determined by the ratio of the elastic moduli of the particles and the matrix. We obtained A and f_{DP} values (A = 15.98 and f_{DP} = 0.083) for bones by fitting Equation 1 with reported elastic modulus values for various animal samples (Table S2†).[6,38] As shown in Fig. S10†, all the data points are located within ±20% of A. The f_{DP} was 0.083, suggesting that approximately 92% of bioapatite in bones contributes to increasing E.

Fig. 4a compares the experimentally obtained E and f_{V} values with the best fitting curve of Equation 1 for the animal bones (Fig. S10†). The data for control samples are in the range of within ± 20% of A, showing that mechanical properties of collagen matrices

mineralized without loading are comparable to those of early-stage animal bones. Interestingly, the increase in E by cyclic strain was even higher than the model prediction, indicating that applying cyclic mechanical loading can effectively enhance the mechanical properties of collagen-based biomaterials. Conversely, under static strain, the increase in E is significantly lower than for other conditions due to an extensive CaP formation on the outer surface of the collagen matrix (Fig. 3d). The outer surface of the collagen matrix is not a desired nucleation site because the CaP nanocrystals can neither adequately bond to the collagen (increasing f_{DP}) nor transfer the load within the matrix (decreasing E). Therefore, an environment that causes permanent mechanical strain in collagen should be avoided in the synthesis of elastic biomaterials. In addition to the low crystalline degree of crystals at the early stage of mineralization, the inclusion of debonded nanocrystals can result in a weak orientation of WAXD data from all strain conditions (Fig. S5†).

Because the term debonded particle is a theoretical concept, f_{DP} cannot be experimentally quantified. Instead, to explain the nonlinear relationship of E and f_V shown in Fig. 6a, we used f_{IS} obtained by analyzing mineralization depths from TEM images (Fig. S7†). Although f_{IS} was estimated from the contrast of the images, thus the value does not exactly represent the mass or volume of the CaP crystals. However, CaP crystals formed only within the inner surface of the matrix can bond with the collagen, thus we assume that f_{IS} should be reversely related to f_{DP}. Therefore, the relative increases in E per f_V ($(E/E_{UN} - 1) / f_V$, corresponding to the slopes of Fig. 4a) and f_{IS} show a linear relationship (Fig. 4b).

The differences in mineral stiffening behavior by loading conditions highlight the importance of both nano- and microscale distribution of CaP nanocrystals on the surfaces and within the matrices in defining tissue-level mechanical properties. Increasing the microscale depth of mineralized layers in vitro is critical for the construction of collagen-based biomaterials with the total mineral content and mechanical properties that are comparable to bones. The nanoscale spatial distribution of CaP nanocrystals (whether tightly bonded with

collagen fibrils or not) influences the effectiveness of mineral inclusion for enhancing mechanical properties. In this study, the evaluation of CaP spatial distribution reasonably explains the differences in mechanical strength between the experimental data and the conventional model predictions based on the total mineral contents.[6,38] In future studies, the role of nanoscale collagen fibril nucleation sites (e.g., fractions of mineralization in the gap regions which can be identified using techniques such as scanning transmission electron microscopy using electron energy loss spectroscopy and high-angle annular dark-field imaging[42]) on macroscale matrix mechanical properties should be explored.

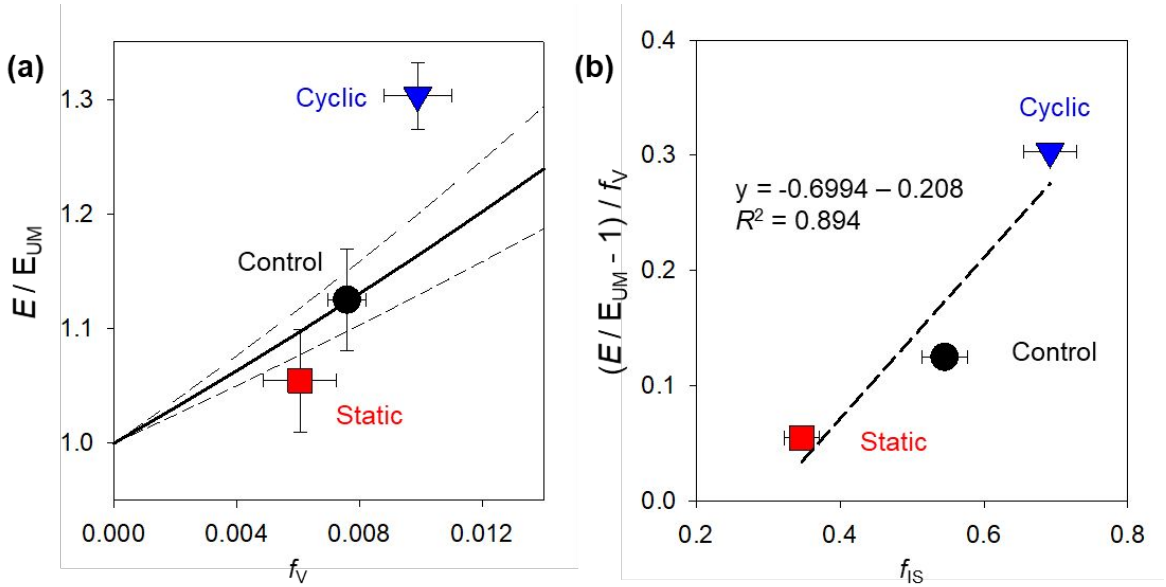

Figure 4. Elastic moduli of mineralized collagen matrices (E) under different loading conditions for 10 h. a) Relative increase in the modulus (E/E_{UN}) vs. volume fraction of mineral in the matrix (f_V). Solid line is Equation 1 with A = 15.98 and f_{DP} = 0.083, based on the best fitting result of data from animal bones (Fig. S10†). Dashed lines show a range of ± 20% of A, where most animal bone data were located. b) Relative increases in the modulus per f_V vs. f_{IS}. The dashed line is a linear fitting of the data. Error bars are standard errors.

3.5. Transport of nucleation precursors in strain-mediated flow

Bone's ability to resist fracture is developed by adapting to repeated loading with varying strain magnitudes and frequencies.[43] Previous studies described how cells in bone modulate their activities by strain-mediated fluid flow in the lacunar-canalicular spaces, by strain-generated potentials, and by fluid shear stress.[12,44] While these biological mechanisms have been studied extensively, the role of strain-mediated fluid flow on the physical chemistry of

biomineralization is poorly understood. The enhanced transport of body fluids by cyclic strain may directly influence mineralization, as implied in our cell-free collagen mineralization system. There are micropores in the extrafibrillar spaces within collagen matrices[10] as well as nanoscale pores known as intrafibrillar gap regions.[45] Deformation of these pore spaces under cyclic strain conditions produces pressure gradients that enhance fluid flow.[12] Increased fluid flow would then increase the delivery of precursor molecules, including Ca^{2+}, HPO_4^{2-}, prenucleation clusters, and/or ACP,[17,21,31] to deeper sites in the collagen matrices. In this study, the transport of body fluid components into collagen matrices under different strain conditions was evaluated using Sirius Red dye observed under confocal microscopy. This red fluorescent molecule (MW: 1,373 g mol^{-1}; $pK_{a1-6} < 2$, $pK_{a7,8} > 13$) stains collagen; therefore, counting fluorescence intensity at different depths of collagen indicates how actively the molecules have diffused into the matrix without interference in diffusion by mineral formation at the exterior of the collagen matrix. The results demonstrated a 40% increase in the penetration depth of the staining molecule under cyclic strain conditions compared to the control condition (Fig. 5). This behavior is consistent with the findings of increased J_s and deeper mineralization depth, which consequently increased the elastic modulus of the matrices after mineralization.

Recent studies have reported the influence of indirect external stimulation (e.g., mimicking the microenvironment induced by cyclic strain in bone) on collagen mineralization. For example, Du et al. showed that applying periodic fluid shear stress to a solution containing dissolved collagen fibrils can promote intrafibrillar mineralization and hierarchical structuring of the fibrils.[46] Our previous study showed that pulsed electrical stimulation could locally boost the diffusion of ionic precursor molecules into microscale spaces, controlling the spatial distribution of CaP minerals within the collagen matrices obtained from demineralized bones.[47] In this study, by successfully applying cyclic strain directly to demineralized bone samples, we demonstrate that the hierarchical collagen

structure is an active template responding to mechanical loading conditions for its mineralization. A better understanding of the physicochemical interactions between collagen and ionic precursors, from nanoscale nucleation to macroscale properties, will contribute to the development of non-invasive treatment of tissue regeneration and the design of a hierarchical bone replacement.

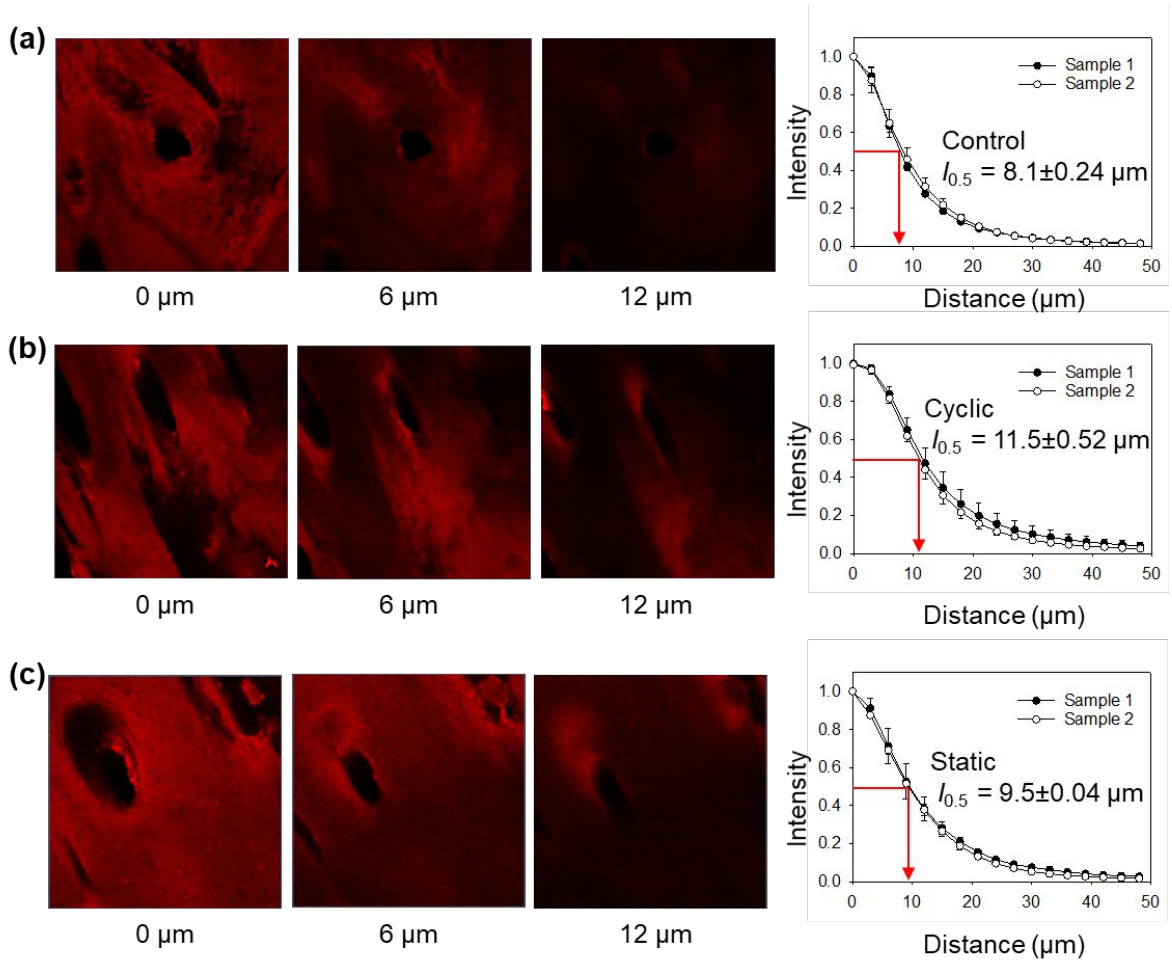

Figure 5. Transport of Sirius Red fluorescent into collagen matrices. Microscope images of confocal sections of collagen matrices at z = 0, 6, 12 μm. Samples experienced different strain conditions (a, control; b, cyclic strain; and c, static strain) in PBS containing Sirius Red for 10 h. Right plots show the average red fluorescence intensities of the images (normalized using the intensity at 0 μm) at different depths. $I_{0.5}$ is the depth position where the intensity reduces to half. Error bars are standard errors from triplicate measurements for randomly selected areas.

4. Conclusion

In this study, we evaluated the influence of cyclic strain on the initial nucleation and crystallization of CaP nanocrystals at the early stages of collagen mineralization. The cyclic

strain condition, simulating mechanical loading from human walking, increased J_s, with deeper inner matrix mineralization. These outcomes resulted from the enhanced transport of precursor molecules in the mineralization solution by strain-mediated flow. The cyclic strain condition significantly influenced the spatial distribution of CaP nanocrystals at the microscale, leading to more inner matrix mineralization. Cyclic mechanical loading effectively overcame the diffusion barriers created by the extracellular matrix, delivering nucleation precursor molecules to locations within the matrix where nuclei formed (e.g., collagen gap regions). Thus, mineralization under cyclic strain increased the E and strength of the matrices more effectively than unloaded or static strain conditions. CaP nanocrystals that formed in the inner matrix of collagen increased E more effectively than particles that formed at the outer surface of the matrix, which cannot transfer load efficiently. We adapted a debonded particle concept to describe how closely were the nanoparticles bonded to collagen fibrils (i.e., nanoscale spatial distribution). By analyzing f_{IS} to represent well-bonded particle fraction, we were able to explain how collagen matrices with a similar total mineral content show different mechanical strength (Fig. 4). By showing enhanced mineralization and elastic moduli of collagen matrices under cyclic loading, our findings highlight new aspects of physiologic loading in bone health and contribute to designing improved hierarchical biomaterials.

Conflicts of interest

There are no conflicts to declare.

Acknowledgements

The authors acknowledge Dr. Spencer Lake and Mr. Ryan Castile (Musculoskeletal Soft Tissue Lab at Washington University in St. Louis) for providing their facilities for tensile testing and freezing leveling of samples. The Nano Research Facility, the Institute of

Materials Science & Engineering, and the Molecular Microbiology Imaging Facility at Washington University in St. Louis provided their facilities for the experiments. We thank Prof. J. Ballard for carefully reviewing the manuscript. The project was supported by the National Science Foundation (DMR-1608545 and DMR-1608554). Use of the Advanced Photon Source (sectors 12-ID-B and 11-ID-B) at Argonne National Laboratory was supported by the U.S. Department of Energy, Office of Science, Office of Basic Energy Sciences, under Contract No. DE-AC02-06CH11357.

References

1 A. L. Boskey, *Elements*, 2007, **3**, 385–391.

2 M. J. Glimcher, *Rev. Mineral. Geochemistry*, 2006, **64**, 223–282.

3 N. Reznikov, R. Shahar and S. Weiner, in *Acta Biomaterialia*, 2014, **10**, 3815–3826.

4 Y. Liu, S. Thomopoulos, C. Chen, V. Birman, M. J. Buehler and G. M. Genin, *J. R. Soc. Interface*, 2014, **11**, 20130835.

5 K. D. Rogers and P. Zioupos, *J. Mater. Sci. Lett.*, 1999, **18**, 651–654.

6 J. D. Currey, *J. Biomech.*, 1988, **21**, 131–139.

7 J. D. Currey, A. Miller, D. C. Phillips and R. J. P. Williams, *Philos. Trans. R. Soc. London. B, Biol. Sci.*, 1984, **304**, 509–518.

8 E. Tanck, G. Hannink, R. Ruimerman, P. Buma, E. H. Burger and R. Huiskes, *J. Anat.*, 2006, **208**, 73–79.

9 D. A. Bailey, H. A. McKay, R. L. Mirwald, P. R. E. Crocker and R. A. Faulkner, *J. Bone Miner. Res.*, 1999, **14**, 1672–1679.

10 S. P. Fritton and S. Weinbaum, *Annu. Rev. Fluid Mech.*, 2009, **41**, 347–374.

11 D. B. Burr, A. G. Robling and C. H. Turner, in *Bone*, 2002, **30**, 781–786.

12 K. Piekarski and M. Munro, *Nature*, 1977, **269**, 80–82.

13 S. W. Donahue, C. R. Jacobs and H. J. Donahue, *Am. J. Physiol. - Cell Physiol.*, 2001, **281**, C1635–C1641.

14 S. D. Tan, T. J. de Vries, A. M. Kuijpers-Jagtman, C. M. Semeins, V. Everts and J. Klein-Nulend, *Bone*, 2007, **41**, 745–751.

15 S. S. Jee, L. Culver, Y. Li, E. P. Douglas and L. B. Gower, *J. Cryst. Growth*, 2010, **312**, 1249–1256.

16 D. Kim, B. Lee, S. Thomopoulos and Y. S. Jun, *Nat. Commun.*, 2018, **9**, 962.

17 D. Kim, B. Lee, S. Thomopoulos and Y.-S. Jun, *Cryst. Growth Des.*, 2016, **16**, 5359–5366.

18 S. S. Jee, T. T. Thula and L. B. Gower, *Acta Biomater.*, 2010, **6**, 3676–3686.

19 Y. Wang, T. Azaïs, M. Robin, A. Vallée, C. Catania, P. Legriel, G. Pehau-Arnaudet, F. Babonneau, M. M. Giraud-Guille and N. Nassif, *Nat. Mater.*, 2012, **11**, 724–733.

20 M. J. Olszta, X. Cheng, S. S. Jee, R. Kumar, Y. Y. Kim, M. J. Kaufman, E. P. Douglas and L. B. Gower, *Mater. Sci. Eng. R Reports*, 2007, **58**, 77–116.

21 F. Nudelman, K. Pieterse, A. George, P. H. H. Bomans, H. Friedrich, L. J. Brylka, P. A. J. Hilbers, G. De With and N. A. J. M. Sommerdijk, *Nat. Mater.*, 2010, **9**, 1004–1009.

22 A. A. Poundarik, A. Boskey, C. Gundberg and D. Vashishth, *Sci. Rep.*, 2018, **8**, 1191.

23 L. E. Bertassoni and M. V Swain, *Connect. Tissue Res.*, 2017, **58**, 414–423.

24 J. Chen, C. Burger, C. V. Krishnan, B. Chu, B. S. Hsiao and M. J. Glimcher, *Macromol. Chem. Phys.*, 2005, **206**, 43–51.

25 Y. S. Jun, B. Lee and G. A. Waychunas, *Environ. Sci. Technol.*, 2010, **44**, 8182–8189.

26 H. J. Ralston, *Neural control of locomotion*, Springer, 1976, pp.77–98.

27 P. J. Ehrlich and L. E. Lanyon, *Osteoporos. Int.*, 2002, **13**, 688–700.

28 Y. Liu, A. G. Schwartz, V. Birman, S. Thomopoulos and G. M. Genin, *Biomech. Model. Mechanobiol.*, 2014, **13**, 973–983.

29 H. Spatz -Ch., E. J. O'Leary and J. F. V. Vincent, *Proc. R. Soc. B Biol. Sci.*, 1996, **263**, 287–294.

30 W. J. Landis, M. J. Song, A. Leith, L. McEwen and B. F. McEwen, *J. Struct. Biol.*, 1993, **110**, 39–54.

31 W. J. E. M. Habraken, J. Tao, L. J. Brylka, H. Friedrich, L. Bertinetti, A. S. Schenk, A. Verch, V. Dmitrovic, P. H. H. Bomans, P. M. Frederik, J. Laven, P. Van Der Schoot, B. Aichmayer,

G. De With, J. J. DeYoreo and N. A. J. M. Sommerdijk, *Nat. Commun.*, 2013, **4**, 39–54.

32 T. Li, A. J. Senesi and B. Lee, *Chem. Rev.*, 2016, **1161**, 11128–11180.

33 F. Bianchi, F. Hofmann, A. J. Smith and M. S. Thompson, *Acta Biomater.*, 2016, **45**, 321–327.

34 G. Beaucage, H. K. Kammler and S. E. Pratsinis, *J. Appl. Crystallogr.*, 2004, **37**, 523–535.

35 F. Zhang, J. Ilavsky, G. G. Long, J. P. G. Quintana, A. J. Allen and P. R. Jemian, *Metall. Mater. Transac. A*, 2010, **41**, 1151–1158.

36 P. Fratzl, N. Fratzl-Zelman, K. Klaushofer, G. Vogl and K. Koller, *Calcif. Tissue Int.*, 1991, **48**, 407–413.

37 M. J. Silva, M. D. Brodt, B. Wopenka, S. Thomopoulos, D. Williams, M. H. M. Wassen, M. Ko, N. Kusano and R. A. Bank, *J. Bone Miner. Res.*, 2006, **21**, 78–88.

38 J. D. Currey, *J. Biomech.*, 2004, **37**, 549–556.

39 H. S. Gupta, J. Seto, W. Wagermaier, P. Zaslansky, P. Boesecke and P. Fratzl, *Proc. Natl. Acad. Sci.,* 2006, **103**, 17741–17746.

40 L. J. Smith, A. C. Deymier, J. J. Boyle, Z. Li, S. W. Linderman, J. D. Pasteris, Y. Xia, G. M. Genin and S. Thomopoulos, *Interface Focus*, 2016, **6**, 20150070.

41 H. Teng, *Int. J. Solids Struct.*, 2010, **47**, 2191–2200.

42 B. Alexander, T. L. Daulton, G. M. Genin, J. Lipner, J. D. Pasteris, B. Wopenka and S. Thomopoulos, *J. R. Soc. Interface*, 2012, **9** , 1774–1786.

43 N. H. Hart, S. Nimphius, T. Rantalainen, A. Ireland, A. Siafarikas and R. U. Newton, *J. Musculoskelet. Neuronal Interact.*, 2017, **17**, 114–139.

44 A. F. van Tol, V. Schemenz, W. Wagermaier, A. Roschger, H. Razi, I. Vitienes, P. Fratzl, B. M. Willie and R. Weinkamer, *Proc. Natl. Acad. Sci.*, 2020, **117**, 32251–32259.

45 A. K. Nair, A. Gautieri, S. W. Chang and M. J. Buehler, *Nat. Commun.*, 2013, **4**, 1724.

46 T. Du, X. Niu, S. Hou, M. Xu, Z. Li, P. Li and Y. Fan, *J. Mater. Chem. B*, 2020, **8**, 2562–2572.

47 D. Kim, B. Lee, B. Marshall, E. Jang, S. Thomopoulos and Y.-S. Jun, *ACS Appl. Bio Mater.*, 2019, **3**, 902–910.